An integral approach to plasma-wall interaction modelling for EU-DEMO

D. Matveev, C. Baumann, J. Romazanov, S. Brezinsek, S. Ratynskaia, L. Vignitchouk, P. Tolias, K. Paschalidis, D. Tskhakaya, M. Komm, et al.

OPEN ACCESS
IOP Publishing | International Atomic Energy Agency
Nuclear Fusion
Nucl. Fusion **64** (2024) 106043 (13pp)
https://doi.org/10.1088/1741-4326/ad73e7

An integral approach to plasma-wall interaction modelling for EU-DEMO

D. Matveev[1,*], C. Baumann[1], J. Romazanov[1,9], S. Brezinsek[1,10], S. Ratynskaia[2], L. Vignitchouk[2], P. Tolias[2], K. Paschalidis[2], D. Tskhakaya[3], M. Komm[3], A. Podolník[3], J. Mougenot[4], Y. Charles[4], R. Delaporte-Mathurin[4,5,11], E. Hodille[5], C. Grisolia[5], F. Montupet-Leblond[5], K. Schmid[6], U. Von Toussaint[6], F. Granberg[7], F. Kporha[7], J. Kovačič[8] and S. Costea[8]

[1] Forschungszentrum Jülich GmbH, Institute of Fusion Energy and Nuclear Waste Management – Plasma Physics, Jülich, 52425, Germany
[2] Space and Plasma Physics—KTH Royal Institute of Technology, SE-10044 Stockholm, Sweden
[3] Institute of Plasma Physics of the CAS, Za Slovankou 3, Prague 8 182 00, Czech Republic
[4] Université Sorbonne Paris Nord, Laboratoire des Sciences des Procédés et des Matériaux, LSPM, CNRS, UPR 3407, F-93430 Villetaneuse, France
[5] CEA, IRFM/GCFPM, F-13108 Saint-Paul-lez-Durance, France
[6] Max Planck Institute for Plasma Physics, Boltzmannstrasse 2, 85748 Garching, Germany
[7] Department of Physics, University of Helsinki, Post-office Box 43, FIN-00014 Helsinki, Finland
[8] Reactor Physics Department, Jožef Stefan Institute, Jamova 39, 1000 Ljubljana, Slovenia
[9] JARA-HPC, Jülich Supercomputing Centre, Forschungszentrum Jülich GmbH, 52425 Jülich, Germany
[10] Heinrich-Heine-Universität Düsseldorf, Mathematisch-Naturwissenschaftliche Fakultät, 40225 Düsseldorf, Germany
[11] Plasma Science and Fusion Center, Massachusetts Institute of Technology, Cambridge, MA 02139, United States of America

E-mail: d.matveev@fz-juelich.de

Received 15 January 2024, revised 24 June 2024
Accepted for publication 27 August 2024
Published 6 September 2024

Abstract

An integral approach to plasma-wall interaction (PWI) modelling for DEMO is presented, which is part of the EUROfusion Theory and Advanced Simulation Coordination activities that were established to advance the understanding and predictive capabilities for the modelling of existing and future fusion devices using a modern advanced computing approach. In view of the DEMO design, the aim of PWI modelling activities is to assess safety-relevant information regarding the erosion of plasma-facing components (PFCs), including its impact on plasma contamination, dust production, fuel inventory, and material response to transient events. This is achieved using a set of powerful and validated computer codes that deal with particular PWI aspects and interact with each other by means of relevant data exchange. Steady state erosion of tungsten PFC and subsequent transport and re-deposition of eroded material are simulated with the ERO2.0 code using a DEMO plasma background produced by dedicated SOLPS-ITER simulations. Dust transport simulations in steady state plasma also rely on the respective SOLPS-ITER solutions and are performed with the MIGRAINe code. In order to improve simulations of tungsten erosion in the divertor of DEMO, relevant high density sheath models are being developed based on particle-in-cell (PIC) simulations with the state-of-the-art BIT code family. PIC codes of the SPICE code family, in turn, provide relevant information on

* Author to whom any correspondence should be addressed.

multi-emissive sheath physics, such as semi-empirical scaling laws for field-assisted thermionic emission. These scaling laws are essential for simulations of material melting under transient heat loads that are performed with the recently developed MEMENTO code, the successor of MEMOS-U. Fuel retention simulations assess tritium retention in tungsten and structural materials, as well as fuel permeation to the coolant, accounting for neutron damage. Simulations for divertor monoblocks of different sizes are performed using the FESTIM code, while for the first wall the TESSIM code is applied. Respective code-code dependencies and interactions, as well as modelling results achieved to date are discussed in this contribution.

Keywords: DEMO, EU-DEMO, plasma-wall interaction, erosion-deposition, transient melting, dust evolution, fuel retention

(Some figures may appear in colour only in the online journal)

1. Introduction

Plasma-wall interaction (PWI) in DEMO will have a strong impact on the lifetime of plasma-facing components (PFCs), reactor safety, and availability of the plant. The critical issues of material erosion and damage, impurity generation, formation and destabilization of deposited layers, and tritium (T) retention are identified. A separate task dedicated to the development of PWI modelling capabilities for DEMO has been established within EUROfusion Theory and Advanced Simulation Coordination [1] activities. This task aims at the critical assessment of safety-relevant information regarding PFC erosion, dust production, fuel inventory, and material response to transient events, such as vertical displacement events (VDEs), thus providing vital input for the DEMO conceptual design evaluation. To achieve this goal, a set of powerful and validated computer codes that deal with particular aspects of PWI is applied and further developed to account for DEMO specific requirements. Different aspects of PWI modelling addressed by the integral approach and corresponding code-code interactions are sketched in figure 1.

The paper is structured as follows. In section 2 the modelling tools and their interactions in view of DEMO PWI studies are described, followed by subsequent sections where preliminary results of respective modelling are presented. Section 3 describes the modelling of steady-state tungsten (W) erosion and re-deposition in DEMO. Limitations of currently applied plasma sheath models and PWI data are discussed in section 4, which introduces auxiliary activities towards improved descriptions of respective PWI aspects. Section 5 covers the topic of fuel retention and permeation in view of safety and tritium self-sufficiency. The potential for transient melting and melt splashing during VDE is addressed in section 6. In the following section 7, the evolution of repetitive plasma discharges in dust inventory, originating either from melt splashing events or from the flaking of deposited layers is presented. Finally, section 8 gives a brief summary of the paper with prospects for improved modelling.

2. Modelling tools

The analysis of steady-state PWI in DEMO is performed with the 3D Monte-Carlo impurity transport code ERO2.0 [2] that represents one of the main building blocks (‘Global PWI in steady-state’) of the interaction diagram in figure 1. ERO2.0 allows modelling of PWI and self-consistent global impurity transport in the entire volume of a reactor-scale device, using a realistic 3D description of all relevant PFCs and comprehensive models for trace particle interactions with plasma and material surfaces. The code has been successfully validated in contemporary devices, such as JET [3], WEST [4], W7-X [5], and applied as a predictive tool for ITER [5, 6].

Material erosion, transport and deposition simulations rely on input data regarding the steady-state plasma, typically considered as a stationary background and provided by specialized simulation tools such as SOLPS-ITER [7]. Further input is local PWI data, such as particle reflection and erosion yields, which are provided by molecular dynamics (MD) simulations and binary collision codes. Among the latter, the SDTrimSP code [8] provides an established reference. While the DEMO plasma background for ERO2.0 is considered to be an external input from other EUROfusion research and modelling activitiesin particular, from the DEMO Central Team [9], the improvement of the local PWI data is part of the integral approach as shown by the respective block in figure 1 and will be discussed in section 4. The way local PWI data affect material erosion is a direct function of plasma sheath characteristics. Self-consistent calculations of the electric field and plasma parameters in the sheath are possible with particle-in-cell (PIC) codes, among which the BIT [10] and SPICE [11] code families represent the state-of-the-art simulations tools. It is expected that in the case of high density plasma in the divertor of DEMO the classical sheath models used in ERO2.0 will be not appropriate due to plasma collisionality, and BIT1 simulations with the recently implemented dressed cross-section model [12] are performed within the integral approach to evaluate the implications of high density sheath physics on PWI. Another application of the BIT1 code is the development of models for dynamic parallel (blob-filament) transport

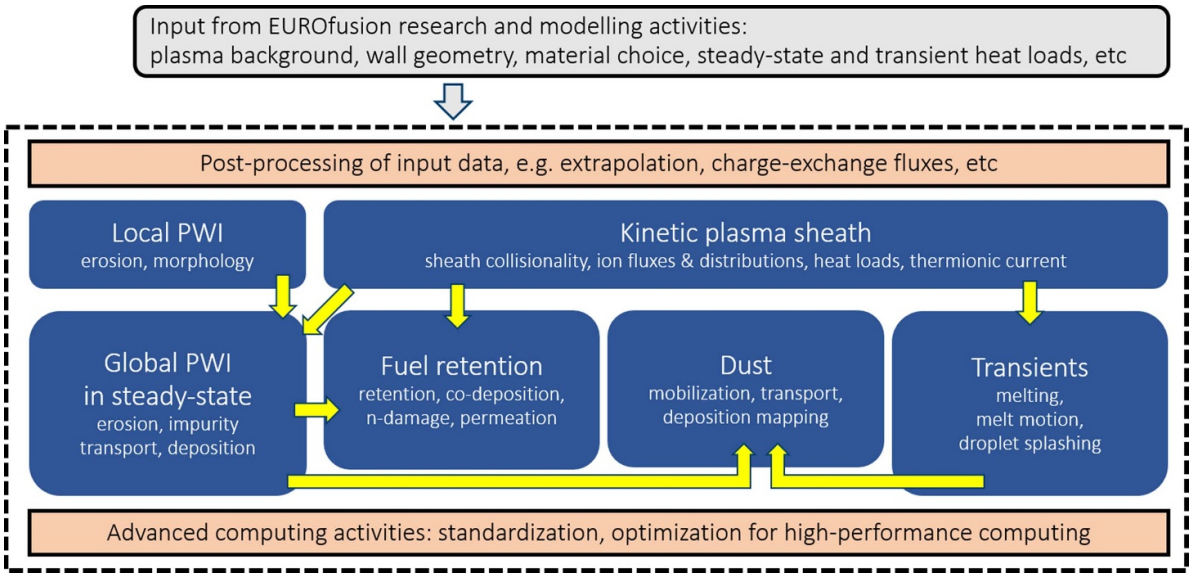

Figure 1. A diagram of different aspects of PWI modelling and their interaction within the integral approach to PWI in DEMO. The 'Kinetic plasma sheath block' implies particle-in-cell (PIC) simulations. The 'Local PWI' block means local scale processes, such as sputtering, while the 'Global PWI' block is the integration of local processes into the global erosion and impurity transport framework. Arrows indicate input/output data exchange between blocks. Not shown in the figure is the link between simulations of transients and the local and global PWI, namely that morphology of re-solidified melt layers can be used in local and global PWI simulations to assess changes in effective erosion and re-deposition rates.

in the scrape-off layer (SOL) [13]. SPICE simulations, in turn, provide crucial information on the multi-emissive sheath characteristics relevant for material melting simulations, describing the field-assisted thermionic emission as a function of magnetic field angle and surface temperature [14, 15], taking also secondary electron emission and electron backscattering into account [16]. These aspects provide the links between the 'Kinetic plasma sheath' and other blocks of the interaction diagram in figure 1.

In-vessel tritium inventory is driven by two essentially different processes, namely implantation and co-deposition. Based on JET experience [17] and predictions for ITER [18], the dominant retention mechanism in the absence of neutron damage of PFC materials is co-deposition. For full-W DEMO, tritium co-deposition with W can be assessed by means of ERO2.0 simulations, following the transport and re-deposition of eroded W and applying available empirical formulae [19] and models [20] for T uptake in deposited layers. Location maps of preferential deposition also serve as input for dust mobilization and transport simulations with the MIGRAINe code [21], thus providing the corresponding links between 'Global PWI', 'Fuel retention' and 'Dust' blocks in the diagram of figure 1. The second pathway for T inventory is retention in the bulk of PFC materials, driven by implantation of energetic T ions and charge-exchange neutrals, diffusion and trapping at ion- and neutron-induced defects. It is expected that n-induced damage distributed throughout the entire bulk of the PFC will be a strong contributor to in-vessel T retention in DEMO. Within this integral approach, bulk retention is addressed by establishing and validating macroscopic rate equation codes TESSIM-X [22] and FESTIM [23]. In addition, the HPC-optimized code RAVETIME is being developed for uncertainty quantification studies in application to T uptake in W and permeation through W armour and across material interfaces.

The expected main plasma transients in DEMO are the regular ramp-up phases, upward and downward VDE and the loss of confinement (H-L transition) [24]. As the DEMO baseline focuses on naturally ELM-free regimes [25], ELMS are not considered within the scope of the presented framework. At the current stage, we also exclude runaway electron beams from consideration, as these represent major off-normal events, while we concentrate on 'regular' transients. In order to protect the first wall during ramp-up phases and VDEs, several so-called sacrificial limiters are proposed to be installed at different specific locations in the plasma chamber [24, 26]. The melting of these limiters in such off-normal events is addressed by the recently developed successor of the MEMOS-U code [27] that is called MEMENTO [28, 29]. The crucial role of thermionic emission in the description of the escaping current and W melting has been already mentioned above—MEMENTO relies on semi-empirical scaling models deduced from SPICE code simulations [16]. Smaller-scale flow features such as strong free-surface deformations and melt ejection are simulated with customized set-ups in ANSYS that solve the coupled multi-phase Navier-Stokes and heat equations using the volume-of-fluid method, with plasma heat and momentum drive as boundary conditions [30]. Such modelling allows the establishment of a catalogue of representative scenarios corresponding to various models of dust/droplet production. Droplet ejection, in turn, provides the second source for in-vessel dust inventory that can be addressed by the MIGRAINe code [21] that incorporates state-of-the-art models for numerous physical processes governing

the heating and lifetime of metallic dust and droplets in full 3D environments. MIGRAINe simulations of in-vessel dust migration for varying initial conditions can be combined to extract quantities of practical interest, such as the overall dust survival rates, dust vaporization maps, the size distribution, and spatial deposition patterns of mobilizable dust.

3. W erosion and re-deposition in steady-state plasma conditions

As a first step, ERO2.0 was successfully applied to full-W ITER as a proxy for DEMO [31]. Parameter studies were performed considering different fractions of seeding impurities in the background plasma. Significant W sputtering by charge-exchange (CX) deuterium (D) atoms in the main chamber was demonstrated, as expected, but depending on conditions, seeded impurities were shown to dominate the erosion, both in the divertor and at the blanket. This modelling, however, had to rely on multiple assumptions and limitations, for example, a pure D plasma background was used without self-consistent feedback of seeding species on the plasma; seeding species were considered to be single-charged and constituted a given constant percentage value of the plasma flux at all wall locations; thermal forces were not included.

As a next step, the 3D CAD geometry of the DEMO design (figure 2(*a*)) and magnetic equilibrium for the DEMO Physics Baseline 2017 [25] were implemented in ERO2.0 with code-internal magnetic shadowing calculations for shaped first wall panels (B field connection length mapping) and successfully validated against PFCFlux [32]. The reason for using the Baseline 2017 data instead of the more recent developments is that only for that equilibrium there exists a self-consistent SOLPS-ITER plasma solution [33] for single null divertor scenario including all charge states of plasma (D) and impurity (He, Ar) species, as well as kinetic analysis of the neutral gas. Though not precisely relevant for full power DEMO operation, this Baseline solution is well suited for testing the relevant functionality and physics of the ERO2.0 code in yet unexplored regimes in preparation for future design-relevant modelling.

The fact that the SOLPS-ITER plasma boundary is limited by the intersection of magnetic field lines in the SOL with divertor target surfaces requires extrapolation of plasma parameters towards the main chamber walls in ERO2.0 simulations. The way this extrapolation is introduced becomes especially critical for DEMO due to the need to bridge large distances, which vary from 10 cm at the inner mid-plane up to about 80 cm above the outer divertor (figure 2(*b*)). In particular in ITER [6], and also for the full-W case simulations [31], a very conservative assumption of constant plasma parameters up to the wall was used. This typically results in the overestimation of wall erosion by ions and reduces the transport of eroded wall materials towards the divertor due to early ionization and prompt local re-deposition. Such an assumption would result in unacceptable W erosion in the main chamber of DEMO due to the overestimation of plasma temperature and inconsistently high ion fluxes to the wall. Therefore, a more benign assumption was adopted, in which the decay of plasma parameters in the SOL was extrapolated exponentially towards the wall with a uniform decay constant of 5 cm. The electron temperature was capped at the lowest value of 2 eV. There are two reasons for this assumption. First, it follows the general conservative approach adopted in ITER simulations [6], as the actual far-SOL plasma characteristics are not reliably known. Second, the Coulomb collision model implementation used within ERO2.0 becomes not accurate for thin and cold plasmas due to vanishing Debye screening and the need to account for longer-range interactions. The parallel Mach number, used for the calculation of the ion flow velocity, was kept constant at the value corresponding to the nearest outer plasma grid node. It has to be noted that the large extrapolation volume introduces significant uncertainties into the modelling so that all presented ERO2.0 results should be considered as preliminary and handled with caution. In particular, no design-relevant conclusions can or should be drawn at this stage.

An important improvement was introduced in the ERO2.0 code to account for charge-state resolved and spatially non-uniform impurity fluxes to the wall, which become highly relevant for DEMO due to the presence of multiple charged Ar and He impurity ions as provided by the SOLPS-ITER solution (figure 3). In particular, compared to initial ERO2.0 simulations for DEMO where the total flux of impurity ions with just an average charge-state was considered, the charge-state resolved data significantly reduces W erosion. This applies mainly to the divertor, where erosion by impurities dominates. In the main chamber, in turn, large distances to the wall and shaping of wall elements lead to reduction of ion fluxes and impact energies so that erosion becomes mostly dominated by CX neutral atoms of fuel isotopes, except for the most plasma-facing apexes of wall elements, mainly inboard, where erosion by impurity ions may still contribute. Accounting for the realistic energy distribution of CX atoms is crucial for proper estimation of wall erosion rates. The standard output of SOLPS-ITER, however, contains only total fluxes and mean energies of neutral atoms to wall segments. The recorded fluxes of neutral atoms contain in fact, both high energy CX atoms and low energy atoms resulting from recycling and dissociation of fuel molecules. Since the sputtering yield has a strongly non-linear energy dependence [34], it would be not correct to apply the total neutral flux with mean energy as reported by SOLPS-ITER data as an erosion source—most of these neutrals have very low energies below the sputtering threshold for W. In general, this is solved by dedicated post-processing of SOLPS-ITER simulations, in which the Monte-Carlo code EIRENE [35] (a module responsible for the neutral transport and atomic and molecular reactions within SOLPS-ITER) is run standalone on top of the stationary plasma solution. In this way one can accumulate sufficient neutral particle statistics for neutral-surface collisions and thus provide the corresponding energy, and preferably also angular distributions of neutral atoms upon wall impact. Up

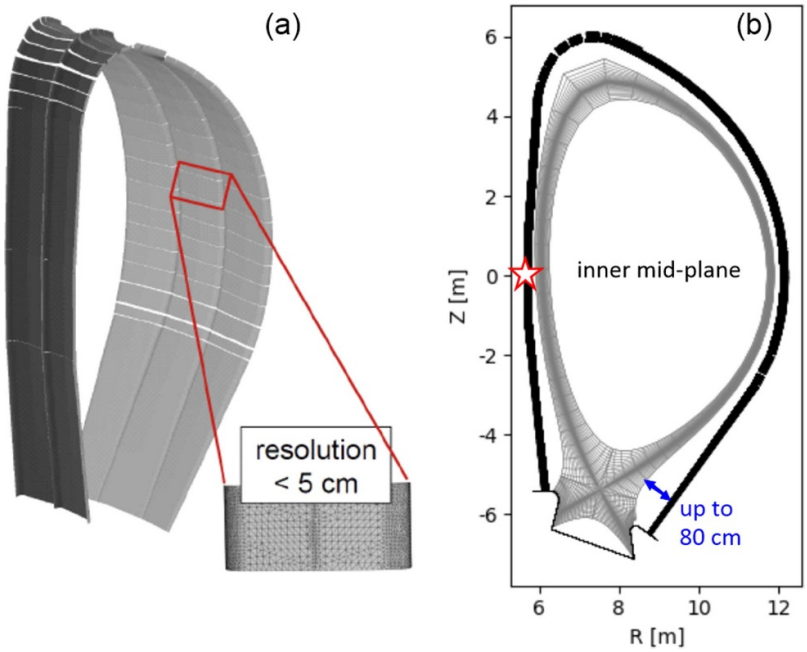

Figure 2. (*a*) DEMO 3D wall geometry in ERO2.0 based on the CAD model, one toroidal sector out of 16 is shown. (*b*) 2D poloidal projection of the wall geometry as used in SOLPS-ITER simulations, the SOLPS-ITER plasma grid is shown, the star symbol indicates the inner mid-plane position that has the smallest gap between the plasma grid and the wall, while the largest gap is shown at the outer wall above the divertor.

to now, this approach has been applied only to a few selected locations on the wall in ITER simulations, for example, for diagnostic mirror studies [36], but is now being also adapted for the DEMO case. Corresponding results will be discussed in future work elsewhere. In the present contribution, an intermediate solution based on the mean energy approach with a constant impact angle of 60° is used for preliminary W erosion-deposition mapping simulations. Corresponding results of ERO2.0 simulations are shown as erosion-deposition maps in figure 4. In the ongoing work, the energy distributions of neutral atoms obtained at multiple locations along the poloidal cross-section of DEMO are incorporated in ERO2.0 simulations to achieve further improvement of the description of erosion by CX neutrals.

The main outcomes from preliminary ERO2.0 simulations can be summarized as follows:

- The main chamber erosion is dominated by neutrals and concentrated mainly around the outer mid-plane.
- Divertor erosion is dominated by Ar ions and self-sputtering is also pronounced.
- There is strong transport of eroded W into the divertor, transport from the divertor to the main chamber is negligible.
- The main W deposition locations are the inner and outer divertor above strike lines, remote areas above the outer divertor (wall gap), and the top of the machine. Despite significant gross erosion in the divertor, the net balance there is positive due to local re-deposition and W source from the main chamber.

4. Plasma sheath and PWI data

BIT1 simulations are performed to address the collisional high density plasma sheath characteristics accounting for atomic and molecular processes. From currently accomplished simulation cases for plasma densities at the sheath entrance up to 5×10^{21} m^{-3} several aspects that can be important for PWI in DEMO are noted. First of all, the ion speed at the sheath entrance turns out to be smaller than the ion sound speed, contrary to the typical assumption used as a boundary condition in SOLPS-ITER simulations, including the DEMO case [33]. Therefore, a consistent simulation of the DEMO plasma background may require a revision of standard Bohm–Chodura conditions [37]. Furthermore, high collisionality leads to energy redistribution between ions and neutrals in the sheath so that not only do the target heat fluxes become dominated by neutrals, but the ion and neutral impact energies and angles are also affected, as well as the ionization probability of sputtered particles within the sheath. For example, the ion angular distribution becomes more isotropic, reflecting that of neutrals (figure 5). Further simulations that take into account seeded Ar impurity and the intrinsic W component due to the sputtering of the divertor target are ongoing, to evaluate their influence on divertor erosion in the high density sheath. The respective energy and angular distributions of impinging ions and neutrals will be incorporated into ERO2.0 simulations at a later stage.

In terms of PWI data, auxiliary activities include investigation by means of MD simulations of W sputtering in the case of supersaturation of the surface layer with hydrogen isotopes. It

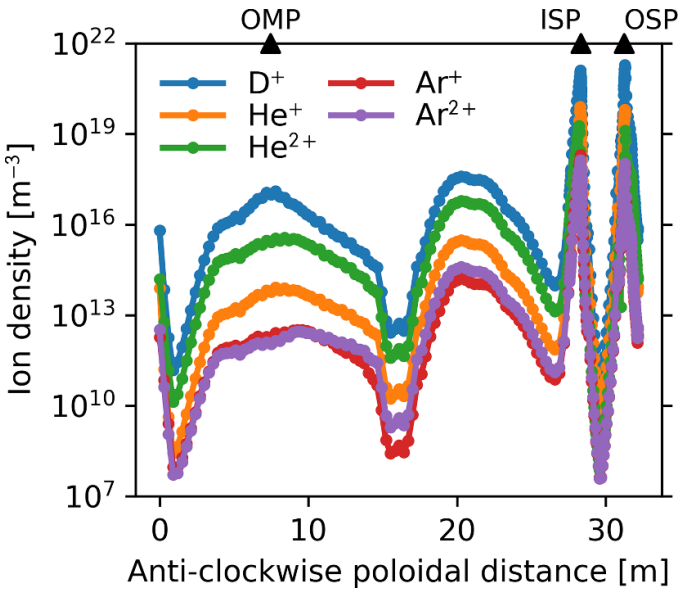

Figure 3. Charge-state and spatially resolved profiles of ion densities for main plasma and impurity species at the wall based on the output of SOLPS-ITER simulations (extrapolated to the wall). Positions of inner/outer strike-points (ISP and OSP) and outer mid-plane (OMP) are marked by respective symbols on the upper plot frame boundary.

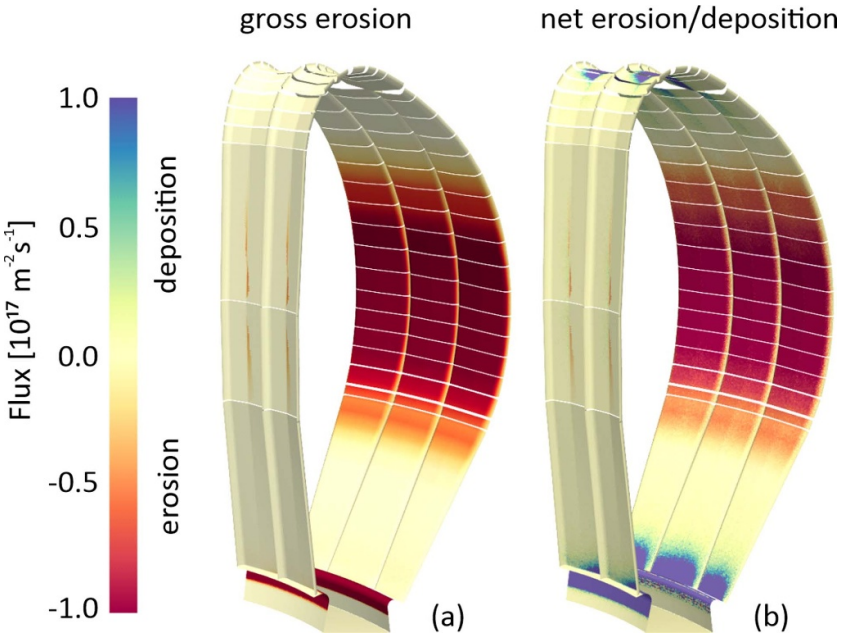

Figure 4. ERO2.0 simulation results for W gross erosion map (*a*) and W net erosion-deposition map (*b*) shown for one (out of 16) toroidal DEMO sector (simulations assume toroidal symmetry of the plasma, and sacrificial limiters are not accounted for in this simulation case).

has been observed experimentally that upon high flux D irradiation a very thin surface layer of W can be saturated with D up to about 10% [38]. While MD simulations of W sputtering by D ions and neutrals under this condition are not yet conclusive, simulations of W bombardment by 200 eV Ar^+ ions, in turn, show an increased W sputtering for the case of supersaturation with D (figure 6), which is explained by the reduction of the W binding energy to the surface when a D atom is present in the vicinity. Detailed studies of these effects as a function of surface orientation will be published in [39].

Further work is ongoing on the implementation of additional options in the 3D version of the SDTrimSP code [40], namely (a) gyromotion for the proper description of ion impact under the influence of electric and magnetic fields, and (b) structured atomic targets for the description of sputtering of crystalline materials. Currently, both options are in the validation phase showing promising results that will be reported in the future. As an example, figure 7 shows validation efforts for the crystal version of SDTrimSP against experimental data [41].

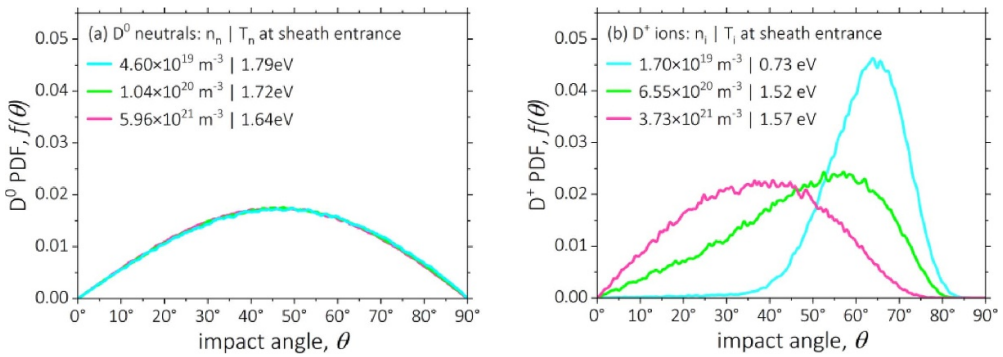

Figure 5. Angular distributions of impacting ions and neutrals (poloidal angle with respect to the surface normal) for different plasma densities at the sheath entrance as given by BIT1 simulations. The angular distributions of impacting ions are strongly affected in the collisional sheath and acquire the shape similar to the distribution of neutrals for the highest density cases (corresponding ion and neutral densities and temperatures at sheath entrance are given in the plot legends).

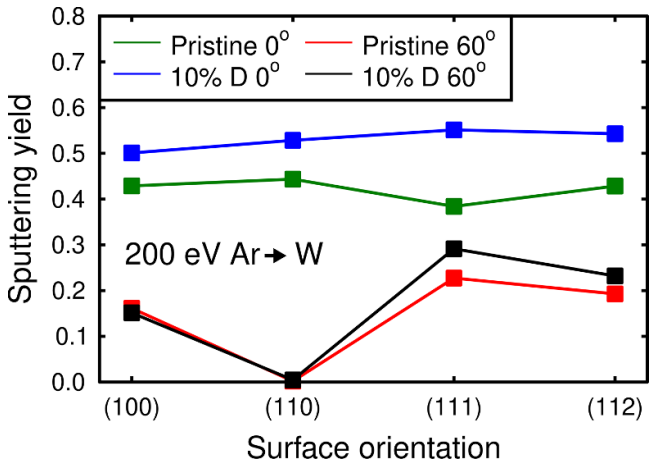

Figure 6. W sputtering yields of a pristine W target and a 10%-D-saturated W target by 200 eV Ar^+ ions for 0° and 60° impact angles and different grain orientations of the W surface simulated with Molecular Dynamics.

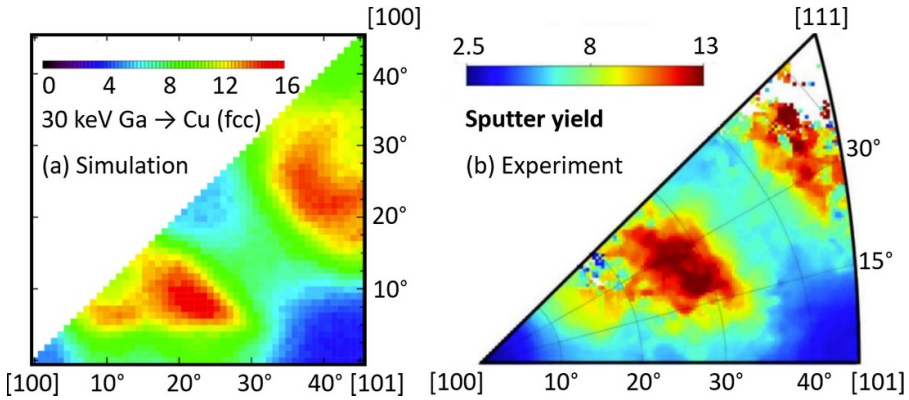

Figure 7. Example of validation of the crystal version of SDTrimSP (*a*) against experimental data [41] (*b*).

5. Fuel retention

Fuel retention studies for DEMO comprise the assessment of tritium permeation and retention at the first wall, in particular in view of tritium self-sufficiency, by means of 1D modelling with the TESSIM-X code and the 3D modelling of tritium retention and permeation to the coolant for divertor monoblocks by FESTIM. For the former, initial estimates have been made in [42]. Recently, this work was revisited using the improved and most recent data on the displacement damage in both W and EUROFER, including the effect of damage stabilization by the presence of hydrogen isotopes [43–46] and available damage annealing data [47]. Refined simulations show a slight increase in the maximum trapped fuel

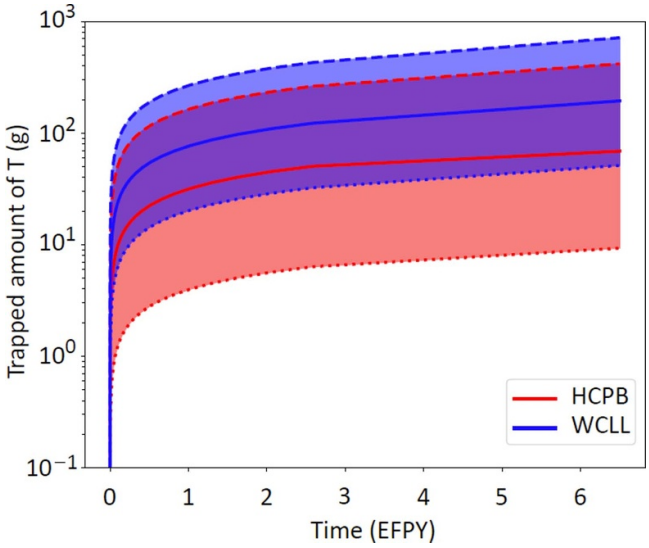

Figure 8. Amount of tritium trapped in the first wall of a DEMO reactor as a function of time in effective full power years (EFPY) of operation for two different breeding blanket concepts: helium cooled pebble bed (HCPB) and water cooled lithium lead (WCLL). The lower limit, median value and upper limit among 48 different cases considered in details in [48] are shown.

concentration in W and a significant reduction of trapped concentration in EUROFER due to damage annealing at DEMO operating temperatures. However, since retention is dominated by the radiation damage in W, the general conclusions of the initial work [42] remain valid. It is shown that, depending on the model parameters, tritium retention can vary by about two orders of magnitude (figure 8). A full analysis with a description of 48 different cases with variation of the coolant concept, particle flux and different boundary conditions towards the coolant is presented in [48]. It has to be noted that the T self-sufficiency analysis presented in [48] relied on a strongly underestimated requirement on the maximum T-wall-loss probability. The corresponding results are being re-evaluated and the corrected implications of T trapping in neutron-induced defects on T self-sufficiency will be the subject of a future paper.

The 1D modelling approach considers the large area of the main chamber to be dominant in view of tritium retention so does not take into account the divertor with its W monoblock design. Fuel retention and permeation in the divertor is, in turn, addressed by the finite elements code FESTIM [49] that is intrinsically capable of working with complex 3D geometries and thus can be applied to monoblock geometry incorporating a cooling pipe channel. The capabilities of the code were demonstrated in application to ITER divertor monoblocks, where simulations were performed in 1D and 2D [50]. A similar approach was adapted to the DEMO monoblock geometry [51]. In this case, not only 2D but also 3D simulations were performed indicating increased D outgassing from the poloidal sides of the monoblock that leads to a reduction of the retained tritium amount by about an order of magnitude compared to the 2D case [52]. Recently, a neutron damage model has been implemented in FESTIM [53] and the simulations were performed, first in 2D, showing very similar trends as TESSIM-X simulations for the first wall, namely that neutron damage significantly increases trapping in W and drastically reduces the permeation to the coolant [54]. Figure 9 shows the considered 2D geometry of the monoblock and how the integral retention per monoblock increases with the damage level. For the highest simulated damage rate of $\eta = 100$ displacements per atom (dpa) over one effective full power year (EFPY), a 17-fold increase in retention compared to the no-damage case ($\eta = 0$) is observed. Practically speaking, neutron-induced defects slow down the outgassing and create a strong permeation barrier due to dominant trapping.

6. Transient melting

Analysis by the DEMO Central Team revealed that the thermal quench (TQ) phase of VDE in DEMO can result in surface heat loads relevant for melting. In particular, for the upper VDE (and the contact with the upper sacrificial limiter, respectively) a maximal perpendicular heat load of 65 GW m^{-2} is predicted, though for a very short duration of only 4 ms. MEMENTO code simulations for this unmitigated heat flux result in unphysical limiter surface temperatures indicating that strong material evaporation will take place. Using a mock-up of vapour shielding relaxes the surface temperature to reasonable values with low sensitivity of the resulting melt thickness on the actual 'restricted' surface temperature being in the range of 4000–6000 K. It is concluded that from heat loads above 5 GW m^{-2} the melt thickness reaches a steady state value of less than 200 μm within the 4 ms TQ duration. Modest melt thickness leads to appreciable viscous damping of the melt pool, which, together with its short lifetime due to re-solidification shortly after heat flux termination, serves for a negligible melt displacement. However, the situation may change if the subsequent current quench (CQ) phase leads to overlapping wetted areas. Unfortunately, a detailed

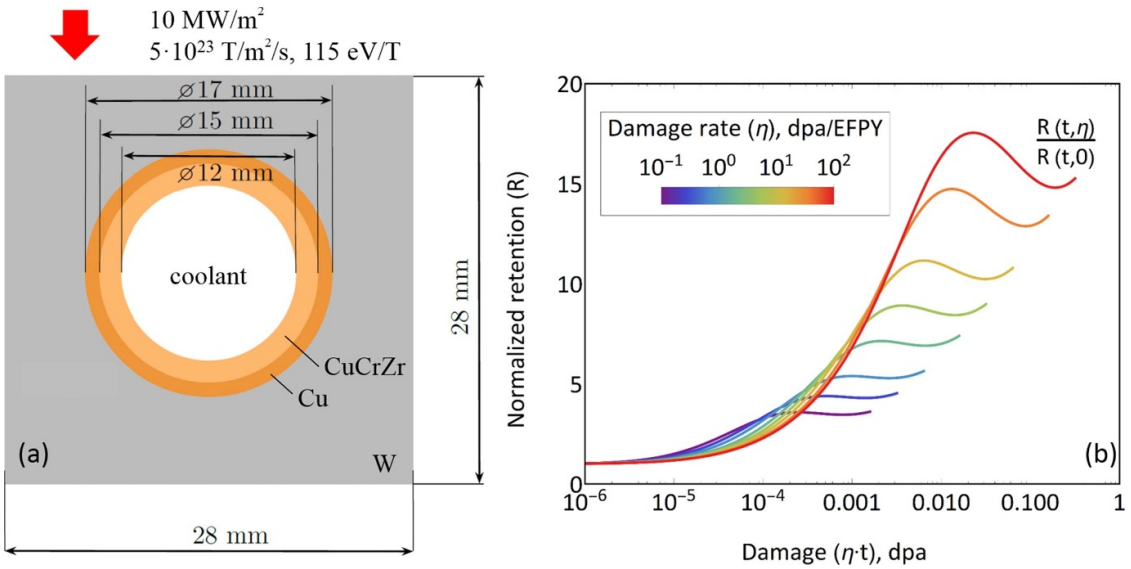

Figure 9. The considered 2D geometry of the ITER-like divertor monoblock (a) and the illustration of the neutron damage effect on the integral tritium retention per monoblock, R, as a function of the damage rate and time. The accumulated damage in displacements per atom (dpa) is a product of the damage rate, η, and time, t. The integral retention per monoblock is normalized to the case without damage ($\eta = 0$ dpa/EFPY).

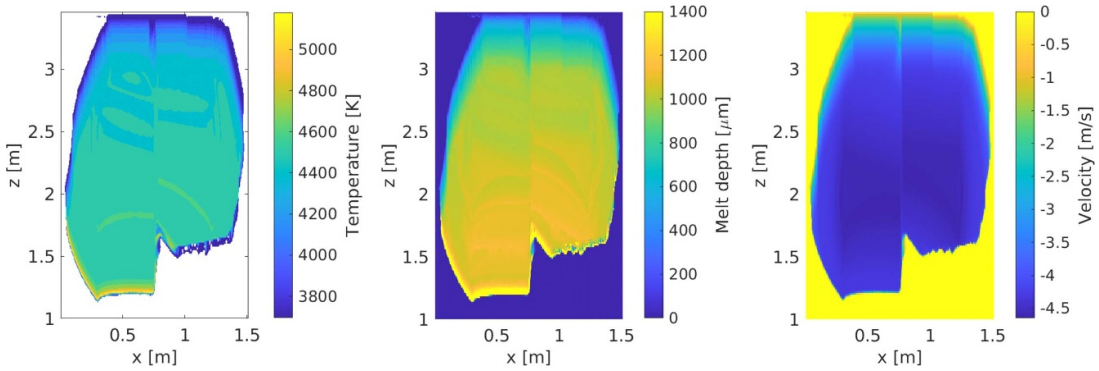

Figure 10. Temperature (left), melt depth (middle) and melt velocity (right) profiles on the upper sacrificial limiter in DEMO during an upper VDE with overlapping thermal quench (TQ) and current quench (CQ) areas (time frame taken 10 ms after CQ). Further details are given in the text.

analysis of CQ heat loads in DEMO is not available at the moment. In the worst case scenario, an ITER-like CQ with a perpendicular heat load of 300 MW m^{-2} and a duration of 200 ms is considered. This moderate but prolonged heat load onto the TQ pre-heated/molten area leads to a sustained melt pool with a longer lifetime and thickness ($\sim$1 mm) as shown in figure 10, thus opening the possibility for a significant melt displacement. The stability analysis for the calculated melt pools includes the Rayleigh-Taylor instability during TQ, the Kelvin-Helmholtz instability due to the near-wall plasma flow during CQ, as well as potential melt splashing when flowing across a sharp PFC edge—a highly likely scenario for a CQ-relevant melt with a characteristic thickness of about 1 mm and speed of 3 m s^{-1}, if a PFC edge can be reached. In this latter case, the estimated Weber number, We, a dimensionless number corresponding roughly to the ratio of the kinetic to surface tension energy of a liquid, is equal to about 60. As an example, in studies of beryllium melt stability in ITER-relevant CQ, significant droplet injection was demonstrated at We = 20 [30]. Further studies will require DEMO-relevant CQ specifications with temporally and spatially varying heat loads and information on the halo current density. With better defined DEMO-specific input, melt stability analysis can be revisited to provide an estimate of characteristic droplet sizes and velocities, which in turn will feed the dust inventory evolution modelling with the MIGRAINe code.

7. Dust inventory evolution

Figure 11 shows the general workflow of, and processes involved [55] in, dust transport simulations with the MIGRAINe code, including the possible connection to the ERO2.0 code simulation results. Three sources of dust are

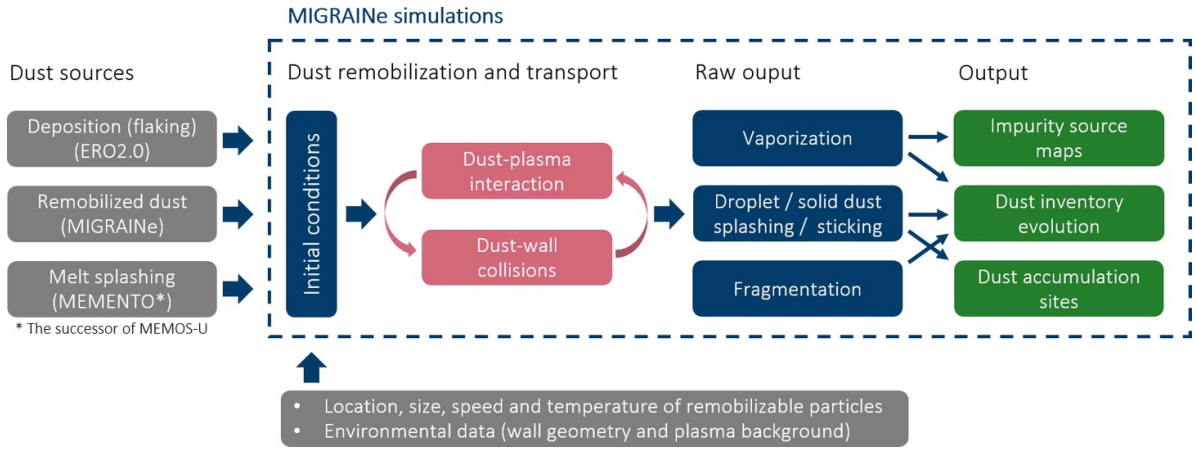

Figure 11. Workflow and processes of dust transport simulations with the MIGRAINe code.

considered: flaking of deposited layers, in particular, based on ERO2.0 deposition maps, dust from previous off-normal events that survived transport through plasma and can be remobilized during plasma ramp-up, for example, and dust produced from melt splashing events (re-solidified droplets). Dust particles that are remobilized according to prescribed conditions and models can undergo interaction with plasma and vessel walls, e.g. vaporization, wall collisions, sticking, etc. It can be noted that the PFC sheath has no effect when modelling dust-wall collisions in MIGRAINe, for three main reasons: the particles of interest are much larger than the sheath thickness; their charge-to-mass ratio is too small to be significantly affected by ambient electric fields; and the mechanical impact forces act on timescales much smaller than plasma forces [55–58]. This explains why there is no link between the 'Kinetic plasma sheath' and 'Dust' blocks in the scheme of figure 1. The final output of dust transport simulations includes the volumetric impurity source maps due to vaporization, overall dust inventory evolution and dust accumulation sites, in particular.

The dynamics of the remobilized dust and the respective dust inventory evolution were first simulated for low-power ITER discharges emulating the reactor start-up environment [59]. Various dust mobilization scenarios varying plasma parameters, dust size distribution, and initial velocity (imposing inverse scaling between initial dust particle radius and injection speed) were studied. It was shown that the dust penetration depth into the plasma, which is governed by the initial dust mobilization speed, has the strongest influence on the results. The dust inventory dynamics were approximated with very high accuracy by a Markov chain model [59], which can be integrated into more global PWI models. As a next step, preliminary simulations for DEMO were performed using the same wall geometry and steady state plasma solution as for ERO2.0 simulations [33]. W dust was injected from the middle of the divertor floor. Three initial dust size distributions were considered (figure 12(*a*)). The main conclusions from the scoping studies for ITER-like discharges [59] are so far confirmed:

- Evaporation material losses are significant (evaporated mass fraction $\sim$10%) only for small particles with a radius below $\sim$25 μm (figure 12(*a*)), localized along the separatrix (figure 13(*a*)). For larger dust particles, evaporation shifts outwards (figure 13(*b*)) due to the centrifugal effect and the evaporated mass fraction accounts only for about 0.05%.
- The preferred dust accumulation site is the outer divertor corner, although dust particles are essentially redistributed along the entire divertor floor and also close to strike points (figure 12(*b*)).

To account for possible dust production from W layers according to preferred deposition locations from ERO2.0 simulations, further dust injection locations are currently being simulated that include divertor target plates, outer divertor baffle regions and the top of the main chamber.

8. Summary

An integral approach to PWI modelling for the European DEMO design is presented. We combine erosion-deposition and impurity transport modelling for the evaluation of the wall lifetime in steady-state plasma with the 3D Monte-Carlo code ERO2.0, which is supported by PIC and PWI modelling activities aimed at improving DEMO specific sheath physics and PWI data, and modelling of PWI response to transient melting with the MEMENTO code. ERO2.0 and MEMENTO simulations help to identify the likely dust production sites via W re-deposition in steady-state plasma and melt droplet injection during off-normal events, so that the in-vessel dust inventory evolution can be modelled with the MIGRAINe code. Last but not least, the critical questions of in-vessel fuel retention, permeation to coolant and overall tritium self-sufficiency are addressed by dedicated macroscopic rate equation codes TESSIM-X and FESTIM, which aim at accounting for neutron-damage of PFC in the burning fusion plasma environment as well as for specific geometry, material and interface structure of PFC components.

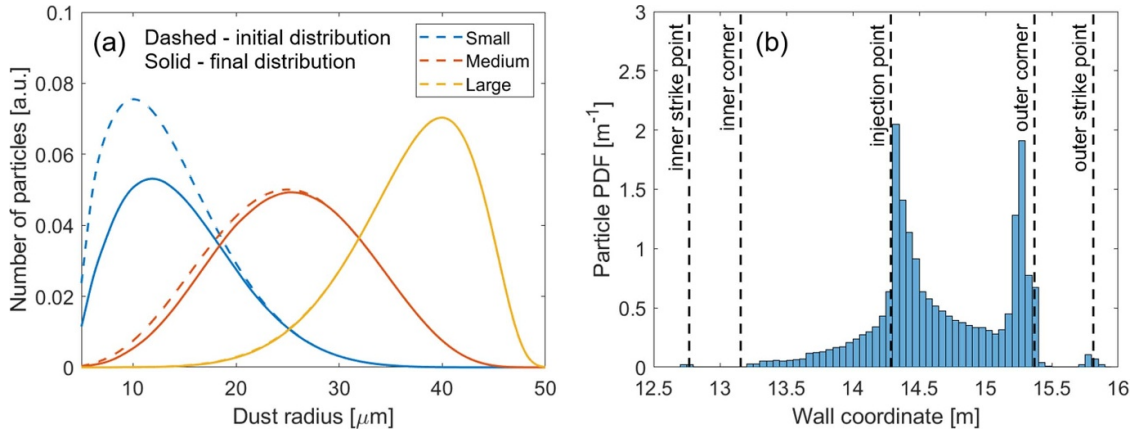

Figure 12. (*a*) Dust size distribution evolution in a single steady state DEMO plasma discharge; the change is due to evaporation of small-sized dust. (*b*) Dust deposition locations (probability distribution function) for the initial dust mobilization from the injection point at the bottom of the divertor flow (figure 13).

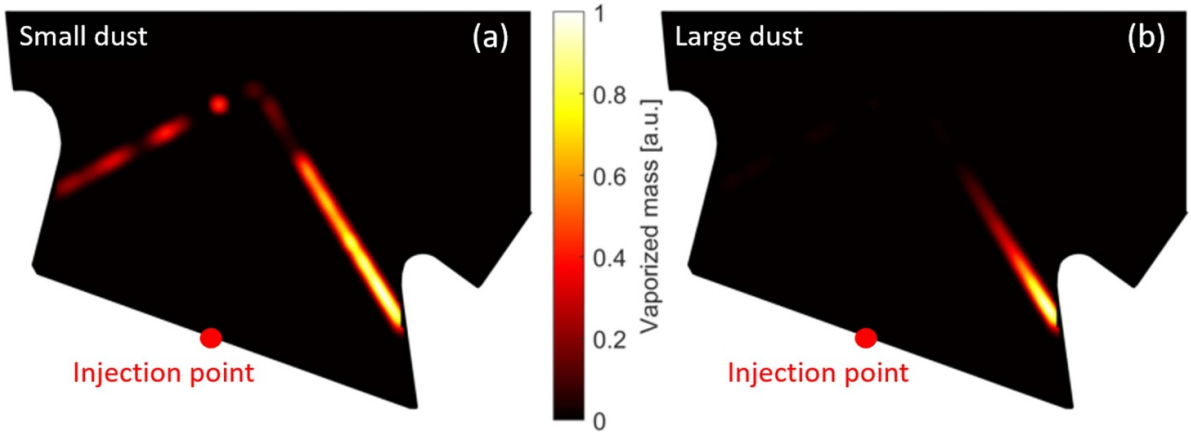

Figure 13. MIGRAINe code simulated evaporation maps for the cases of 'small' (*a*) and 'large' (*b*) dust particle distributions (figure 12(*a*)) for the indicated injection location at the bottom of the divertor floor. The colour map is scaled to the integral value of unity for each plot. In reality, the evaporated mass fraction is 10% for the 'small' dust and 0.05% for the" large" dust, which means a factor 200 lower integral intensity level in the case of 'large' dust (*b*).

In terms of wall lifetime simulations for steady state plasma operation in DEMO, the identified critical aspects are as follows (a) the large wall gap, i.e. the distance between the plasma solution domain and the actual wall profile, which calls for improved SOLPS-ITER simulations with the so-called extended grid option that became publicly available only recently; and (b) the energy and angular resolved CX neutrals data that can be obtained by post-processing the plasma solution using high statistics standalone simulations with the EIRENE code. Parallel to that, the description of the sheath physics in the case of high density divertor plasma with non-negligible collisionality effects is being thoroughly revisited by means of high fidelity PIC simulations. In particular, possible deviation of the parallel flow velocity at the sheath entrance from the ion sound speed velocity calls for further investigations, as this represents a challenge for the standard boundary conditions in edge plasma codes such as SOLPS-ITER. In addition, possible reduction of prompt re-deposition of eroded tungsten can become an issue due to deeper penetration of W impurity into plasma. The data on PWI processes such as sputtering and the capabilities of relevant codes are being improved, an example for which is the sputtering of W with a D-supersaturated surface layer. Fuel retention simulations suggest an extremely strong role of neutron damage of W PFC on fuel inventory with implications on permeation and, potentially, tritium extraction that may impact the fuel cycle. Simulations of transient melting during VDE identify overlapping TQ and CQ heat loaded areas as a possibly critical scenario, leading to significant melting of sacrificial limiters and a potential for melt splashing, especially in the case of melt flow across PFC edges, thus serving as a source for dust production via droplet ejection. Preliminary MIGRAINe simulations confirm the conclusions from previous studies with ITER-like plasmas and will eventually allow us to determine the dust accumulation sites by tracing the dust remobilized from preferred initial dust accumulation locations as identified by means of ERO2.0 simulations and the melt droplets originating from off-normal events.

Acknowledgments

This work has been carried out within the framework of the EUROfusion Consortium, funded by the European Union via the Euratom Research and Training Programme (Grant Agreement No 101052200—EUROfusion). Views and opinions expressed are however those of the author(s) only and do not necessarily reflect those of the European Union or the European Commission. Neither the European Union nor the European Commission can be held responsible for them.

The authors gratefully acknowledge the computing time granted by the *JARA Vergabegremium* and provided on the JARA Partition part of the supercomputer JURECA [60] at Forschungszentrum Jülich.

ORCID iDs

D. Matveev https://orcid.org/0000-0001-6129-8427
C. Baumann https://orcid.org/0000-0001-7712-5379
J. Romazanov https://orcid.org/0000-0001-9439-786X
S. Brezinsek https://orcid.org/0000-0002-7213-3326
S. Ratynskaia https://orcid.org/0000-0002-6712-3625
L. Vignitchouk https://orcid.org/0000-0001-7796-1887
P. Tolias https://orcid.org/0000-0001-9632-8104
K. Paschalidis https://orcid.org/0009-0001-7333-5544
D. Tskhakaya https://orcid.org/0000-0002-4229-0961
M. Komm https://orcid.org/0000-0001-8895-5802
A. Podolník https://orcid.org/0000-0003-1237-8812
J. Mougenot https://orcid.org/0000-0001-7397-0102
R. Delaporte-Mathurin https://orcid.org/0000-0003-1064-8882
E. Hodille https://orcid.org/0000-0002-0859-390X
C. Grisolia https://orcid.org/0000-0002-3038-9593
F. Montupet-Leblond https://orcid.org/0000-0001-7199-1751
U. Von Toussaint https://orcid.org/0000-0002-8867-1014
F. Granberg https://orcid.org/0000-0001-9058-5652
F. Kporha https://orcid.org/0009-0000-7498-168X
J. Kovačič https://orcid.org/0000-0001-7894-9185
S. Costea https://orcid.org/0000-0003-0594-0555

References

[1] Litaudon X. *et al* 2022 *Plasma Phys. Control. Fusion* **64** 034005
[2] Romazanov J. *et al* 2017 *Phys. Scr.* **T170** 014018
[3] Romazanov J. *et al* 2019 *Nucl. Mater. Energy* **18** 331–8
[4] Di Genova S. *et al* 2023 *Nucl. Mater. Energy* **34** 101340
[5] Romazanov J. *et al* 2024 *Nucl. Fusion* **64** 086016
[6] Romazanov J. *et al* 2022 *Nucl. Fusion* **62** 036011
[7] Wiesen S. *et al* 2015 *J. Nucl. Mater.* **463** 480–4
[8] Mutzke A. *et al* 2019 *Max-Planck-Institut für Plasmaphysik* IPP–2019–02 (available at: https://hdl.handle.net/21.11116/0000-0002-F6AE-5)
[9] Federici G., Baylard C., Beaumont A. and Holden J. 2021 *Fus. Eng. Des.* **173** 112960
[10] Tskhakaya D. 2017 *Plasma Phys. Control. Fusion* **59** 114001
[11] Komm M., Ratynskaia S., Tolias P., Cavalier J., Dejarnac R., Gunn J.P. and Podolnik A. 2017 *Plasma Phys. Control. Fusion* **59** 094002
[12] Tskhakaya D. 2023 *Eur. Phys. J.* D **77** 135
[13] Costea S., Kovačič J., Tskhakaya D., Schrittwieser R., Gyergyek T. and Popov T.K. 2021 *Plasma Phys. Control. Fusion* **63** 055016
[14] Komm M., Tolias P., Ratynskaia S., Dejarnac R., Gunn J.P., Krieger K., Podolnik A., Pitts R.A. and Panek R. 2017 *Phys. Scr.* **T170** 014069
[15] Komm M., Ratynskaia S., Tolias P. and Podolnik A. 2020 *Nucl. Fusion* **60** 054002
[16] Tolias P., Komm M., Ratynskaia S. and Podolnik A. 2023 *Nucl. Fusion* **63** 026007
[17] Brezinsek S. *et al* 2013 *Nucl. Fusion* **53** 083023
[18] Schmid K., Krieger K., Lisgo S.W., Meisl G. and Brezinsek S. 2015 *J. Nucl. Mater.* **463** 66–72
[19] de Temmerman G. and Doerner R.P. 2009 *J. Nucl. Mater.* **389** 479–83
[20] Krat S., Prishvitsyn A.S., Vasina Y.A., Gasparyan Y.M. and Pisarev A.A. 2020 *Nucl. Mater. Energy* **24** 100763
[21] Vignitchouk L., Tolias P. and Ratynskaia S. 2014 *Plasma Phys. Control. Fusion* **56** 095005
[22] Schmid K., Bauer J., Schwarz-Selinger T., Markelj S., Toussaint U.V., Manhard A. and Jacob W. 2017 *Phys. Scr.* **T170** 014037
[23] Delaporte-Mathurin R., Hodille E.A., Mougenot J., Charles Y. and Grisolia C. 2019 *Nucl. Mater. Energy* **21** 100709
[24] Vizvary Z. *et al* 2020 *Fus. Eng. Design* **158** 111676
[25] Siccinio M., Graves J.P., Kembleton R., Lux H., Maviglia F., Morris A.W., Morris J. and Zohm H. 2022 *Fus. Eng. Des.* **176** 113047
[26] Maviglia F. *et al* 2021 *Nucl. Mat. Energy* **26** 100897
[27] Ratynskaia S., Thorén E., Tolias P., Pitts R.A., Krieger K., Vignitchouk L. and Iglesias D. 2020 *Nucl. Fusion* **60** 104001
[28] Ratynskaia S., Paschalidis K., Tolias P., Krieger K., Corre Y., Balden M., Faitsch M., Grosjean A., Tichit Q. and Pitts R.A. 2022 *Nucl. Mater. Energy* **33** 101303
[29] Paschalidis K., Ratynskaia S., Lucco Castello F. and Tolias P. 2023 *Nucl. Mat. Energy* **37** 101545
[30] Vignitchouk L., Ratynskaia S., Pitts R.A. and Lehnen M. 2023 *Nucl. Fusion* **63** 016004
[31] Eksaeva A., Kirschner A., Romazanov J., Brezinsek S., Linsmeier C., Maviglia F., Siccinio M. and Ciattaglia S. 2022 *Phys. Scr.* **97** 014001
[32] Firdaouss M., Riccardo V., Martin V., Arnoux G. and Reux C. 2013 *J. Nucl. Mater.* **438** S536–9
[33] Subba F., Coster D.P., Moscheni M. and Siccinio M. 2021 *Nucl. Fusion* **61** 106013
[34] Behrisch R. and Eckstein W. ed 2007 *Sputtering by Particle Bombardment* (*Topics in Applied Physics vol 110*) pp 33–187 (Springer)
[35] Reiter D., Baelmans M. and Börner P. 2005 *Fusion Sci. Technol.* **47** 172–86
[36] Rode S. *et al* 2024 *Nucl. Fusion* **64** 086032
[37] Stangeby P.C. 1999 *The Plasma Boundary of Magnetic Fusion Devices* (Institute of Physics Publishing)
[38] Gao L., Jacob W., von Toussaint U., Manhard A., Balden M., Schmid K. and Schwarz-Selinger T. 2017 *Nucl. Fusion* **57** 016026
[39] Kporha F. *et al* 2024 Sputtering of deuterium decorated tungsten surfaces by argon: a molecular dynamics study *J. Nucl. Mater.* submitted
[40] Von Toussaint U., Mutzke A. and Manhard A. 2017 *Phys. Scr.* **T170** 014056
[41] Balden M., Schlueter K., Dhard D., Bauer P., Nilsson R., Granberg F., Nordlund K. and Hobler G. 2023 *Nucl. Mater. Energy* **37** 101559
[42] Arredondo R., Schmid K., Subba F. and Spagnuolo G.A. 2021 *Nucl. Mater. Energy* **28** 101039

[43] Pecovnik M., Schwarz-Selinger T. and Markelj S. 2021 *J. Nucl. Mater.* **550** 152947
[44] Markelj S., Pečovnik M., Schwarz-Selinger T. and Kelemen M. 2022 *Phys. Scr.* **97** 024006
[45] Schmid K., Schwarz-Selinger T. and Arredondo R. 2023 *Nucl. Mater. Energy* **34** 101341
[46] Schmid K., Schwarz-Selinger T. and Theodorou A. 2023 *Nucl. Mater. Energy* **36** 101494
[47] Theodorou A., Schmid K. and Schwarz-Selinger T. 2024 *Nucl. Mater. Energy* **38** 101595
[48] Schmid K., Schwarz-Selinger T., Arredondo R., Theodorou A. and Pomella Lobo T. 2024 *Nucl. Fusion* **64** 076056
[49] Delaporte-Mathurin R., Dark J., Ferrero G., Hodille E.A., Kulagin V. and Meschini S. 2024 *Int. J. Hydrog. Energy* **63** 786
[50] Hodille E. *et al* 2021 *Nucl. Fusion* **61** 126003
[51] You J.H. *et al* 2022 *Fus. Eng. Des.* **175** 113010
[52] Delaporte-Mathurin R., Chochoy R., Mougenot J., Charles Y., Hodille E.A. and Grisolia C. 2024 *Nucl. Fusion* **64** 026003
[53] Dark J., Mathurin D., Selinger T. S., Hodille E. A., Mougenot J., Charles Y. and Grisolia C. 2024 *Nucl. Fusion* **64** 086026
[54] Hodille E. 2023 *et al Presented at the 15th Int. Symp. on Fusion Nuclear Technology (ISFNT-15)* (*Las Palmas De Gran Canaria, Spain*)
[55] Ratynskaia S. *et al* 2022 *Rev. Mod. Plasma Phys.* **6** 20
[56] Ratynskaia S., Vignitchouk L. and Tolias P. 2022 *Plasma Phys. Control. Fusion* **64** 044004
[57] Shalpegin A. *et al* 2015 *Nucl. Fusion* **55** 112001
[58] Tolias P., Ratynskaia S., Shalpegin A., Vignitchouk L., Brochard F., De Angeli M. and van der Meiden H. 2017 *Nucl. Mater. Energy* **12** 524
[59] Vignitchouk L., Paschalidis K., Ratynskaia S., Tolias P. and Pitts R.A. 2023 *Plasma Phys. Control. Fusion* **65** 015014
[60] Thörni P. 2021 JURECA: data centric and booster modules implementing the modular supercomputing architecture at Jülich supercomputing centre *J. Large-scale Res. Facilities* **7** A182